Plasma impact on black hole shadow and gravitational weak lensing for Schwarzschild-like black hole*

Weiqiang Yang (杨伟强)[1†] Alloqulov Mirzabek[1,2,3,4‡] Abdujabbarov Ahmadjon[5,1,,6§] Ahmedov Bobomurat[1,7,8¶]
Chengxun Yuan (袁承勋)[1♯] Chen Zhou (周晨)[1¶]

[1]School of Physics, Harbin Institute of Technology, Harbin 150001, China
[2]University of Tashkent for Applied Sciences, Tashkent 100149, Uzbekistan
[3]Department of Physics, New Uzbekistan University, Movarounnahr str. 1, Tashkent 100000, Uzbekistan
[4]Tashkent State Technical University, Tashkent 100095, Uzbekistan
[5]Institute of Fundamental and Applied Research, National Research University TIIAME, Kori Niyoziy 39, 100000 Tashkent, Uzbekistan
[6]Andijan State University, Universitet Str. 129, 170100 Andijan, Uzbekistan
[7]Institute of Theoretical Physics, National University of Uzbekistan, Tashkent 100174, Uzbekistan
[8]Institute for Advanced Studies, New Uzbekistan University, Tashkent 100000, Uzbekistan

Abstract: This article delves into the observational properties of a Schwarzschild-like black hole (BH). Initially, the research provides a succinct examination of the spacetime geometry and the configuration of its horizon. Furthermore, we study the photon dynamics around the Schwarzschild-like BH in the presence of plasma using the Hamiltonian formalism. We found that the photon sphere radii increase under the influence of plasma frequency and vice versa for the spacetime parameters. Further exploration is dedicated to understanding how plasma affects the shadow of the BH, and we find that the radius of the BH shadow shrinks with the rise of the ξ parameter and plasma frequency. We then turn to constraining the spacetime parameters and the plasma frequency by using the observational data released by the Event Horizon Telescope (EHT) collaboration for M87* and Sgr A*. Additionally, the research scrutinizes the phenomenon of gravitational weak lensing in the vicinity of a Schwarzschild-like BH, considering both uniform and non-uniform plasma scenarios. The outcomes demonstrate that the angle of deflection increases under the influence of a uniform plasma frequency, whereas the opposite is true for non-uniform plasma. In both scenarios, a rise in the spacetime parameters results in a decrease in the deflection angle. Finally, we investigate the magnification of the gravitationally lensed image. The effect of the spacetime parameters and plasma frequencies on the total magnification is the same as in the deflection angles.

Keywords: black hole, black hole shadow, gravitational weak lensing, plasma

DOI: 10.1088/1674-1137/ae66d2 **CSTR:** 32044.14.ChinesePhysicsC.50075107

I. INTRODUCTION

The past decade has witnessed remarkable progress in black hole (BH) astrophysics, transforming these objects from purely theoretical constructs into observable laboratories for testing gravity in the strong-field regime. The groundbreaking first imaging of the supermassive BHs M87* and Sgr A* by the Event Horizon Telescope (EHT) collaboration [1−3] provided direct visual evidence of BH shadows, while the detection of gravitational waves from binary BH mergers by LIGO and VIRGO [4] opened a new window for probing the dynamics of compact objects. The aforementioned observational breakthroughs stimulated extensive theoretical investigations aimed at constraining deviations from the Kerr paradigm and testing alternative theories of gravity [5−8].

Despite the empirical successes of classical general relativity (GR), fundamental theoretical issues remain unresolved. The singularity theorems established by Roger Penrose [9] demonstrate that, under reasonable physical assumptions, gravitational collapse inevitably leads to the formation of singularities where curvature invariants di-

Received 17 March 2026; Accepted 23 April 2026; Accepted manuscript online 24 April 2026
* This research is funded by the National Natural Science Foundation of China (NSFC) (U2541210)
† E-mail: 25s011087@stu.hit.edu.cn
‡ E-mail: malloqulov@gmail.com (Corresponding authors)
§ E-mail: ahmadjon@astrin.uz
¶ E-mail: ahmedov@astrin.uz
♯ E-mail: yuancx@hit.edu.cn (Corresponding authors)
¶ E-mail: chenzhou@hit.edu.cn (Corresponding authors)

verge and classical physics breaks down. This indicates that GR is incomplete at extreme energy scales, necessitating the incorporation of quantum gravity effects to resolve these pathological features.

Among the various approaches to quantum gravity, the asymptotic safety scenario [10−12] emerged as a compelling framework. This approach proposes that gravity is non-perturbatively renormalizable due to the existence of a non-trivial ultraviolet fixed point that governs the high-energy behavior of the theory. The functional renormalization group provides a systematic tool to investigate the running of gravitational couplings with the energy scale, revealing a characteristic scale dependence of Newton's constant. A powerful phenomenological method to incorporate quantum gravity effects into classical spacetime geometries is the renormalization group improvement procedure [13−15]. This technique utilizes the running of couplings to construct effective metrics that interpolate between the classical infrared regime and the quantum-dominated ultraviolet regime. Recently, the authors of Ref. [16] constructed an explicit renormalization group improved Schwarzschild-like BH spacetime. This new solution exhibits a scale-dependent Newton constant $G(r)$ that interpolates between the classical value G_0 at large distances and a running coupling in the ultraviolet, yielding a regular spacetime with a de Sitter-like core while preserving the asymptotic Schwarzschild structure.

An essential aspect of testing such geometries lies in understanding their observational signatures, which are the BH shadow and weak gravitational lensing. In realistic astrophysical environments, BHs are typically surrounded by various forms of matter, among which plasma constitutes a ubiquitous component. The presence of plasma significantly modifies the propagation of electromagnetic waves, introducing a frequency-dependent effective mass for photons and altering their trajectories compared to vacuum propagation [17−19]. This plasma-induced modification of the geodesic structure provides an additional probe of both the background spacetime and the properties of the surrounding medium [20−23]. To this day, there are different types of studies that have investigated the BH shadow and gravitational weak lensing around compact objects [24−56]. While the above works focused on analytical prediction of shadow shapes, more recent studies have combined general relativistic magnetohydrodynamic (GRMHD) simulations with general relativistic radiative transfer (GRRT) to model realistic accretion flows and emission processes. These simulations show that plasma physics and flow morphology can influence the observed shadow size and asymmetry [57−65]. In this work, we aim to study the photon dynamics around the Schwarzschild-like BH [16] surrounded by plasma using the Hamiltonian formalism, together with the BH shadow and the gravitational weak lensing. Moreover, we take constraints of the spacetime parameters and the plasma frequency using the observational data for M87* and Sgr A*, in spite of their estimation as rotating BHs. Indeed, in real astrophysical scenarios, for instance, energy extraction mechanisms, jet formation, etc., spin plays a key role. Also, the spin would break the spherical symmetry of the BH shadow, leading to a prolate or oblate distortion. Our use of a Schwarzschild-like metric was intended as a foundational non-rotating baseline to isolate the impact of the spacetime parameters without the added geometric complexities of frame-dragging.

The structure of this paper is organized in the following way. In Section II, we review the spacetime of the Schwarzschild-like BH, including the event horizon structure. In addition, we investigate the motion of a photon around the BH surrounded by plasma using the Hamiltonian formalism. The impact of the plasma on the radii of the photon sphere and the BH shadow is explored in this part, together with the constraint values of the spacetime parameters and plasma frequency by using the EHT collaboration results. The weak gravitational lensing and the magnification of the gravitationally lensed images are studied in Sections III and IV, respectively. Finally, we summarize our conclusions and discussions in Section V. Throughout this work, we adopt natural units with $c=\hbar=1$ and the metric signature $(-,+,+,+)$.

II. PLASMA IMPACT ON BLACK HOLE SHADOW

A. Photon dynamics around black hole surrounded by plasma

We consider the spacetime of the Schwarzschild-like BH in the following form

$$\mathrm{d}s^2=-f(r)\mathrm{d}t^2+\frac{\mathrm{d}r^2}{f(r)}+r^2(\mathrm{d}\theta^2+\sin^2\theta\mathrm{d}\phi^2), \tag{1}$$

where

$$f(r)=1-\frac{4Mr^2}{\xi^2(\gamma M+r)+\sqrt{\xi^4(\gamma M+r)^2+4r^6}}. \tag{2}$$

The metric function includes the ξ and γ parameters, which refer to the cutoff scale and interpolation parameters, respectively. It is worth noting that we can recover the standard Schwarzschild spacetime when the ξ parameter tends to zero (see Ref. [13]). In Fig. 1, we plot the radial dependence of the metric function for different values of the spacetime parameters. By solving $f(r)=0$, we can find the event horizon radii, and we plot the radius of

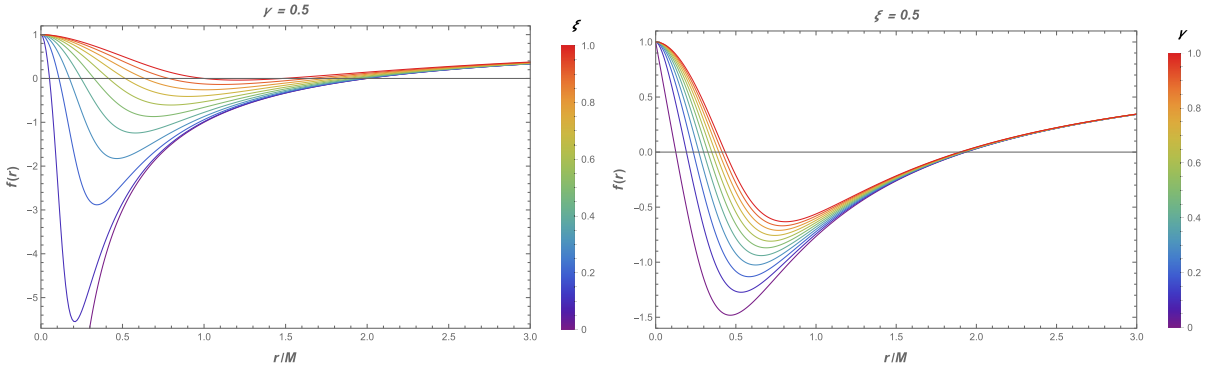

Fig. 1. (color online) The plot shows the radial dependence of the metric function for different values of the ξ parameter (left panel) and the γ parameter (right panel). Here, we set $\gamma = 0.5$ and $\xi = 0.5$ for the left and right panels, respectively.

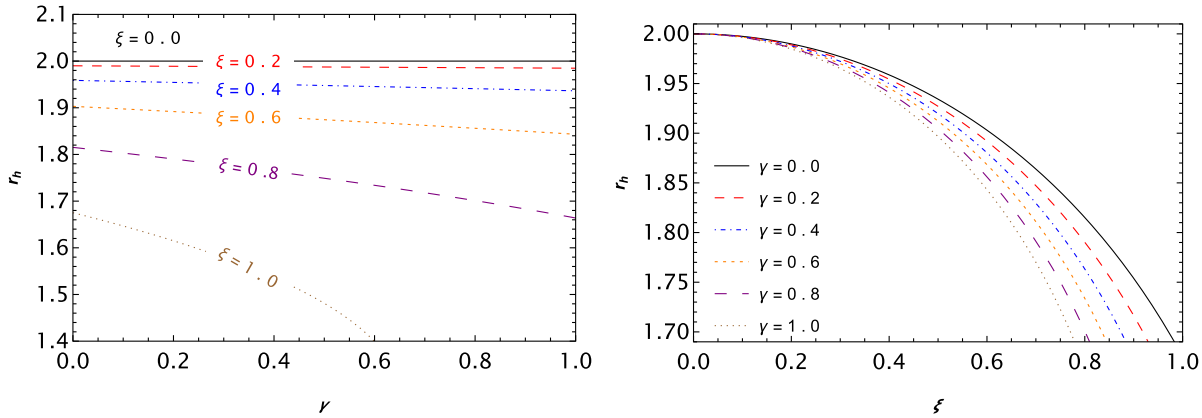

Fig. 2. (color online) The plot illustrates the dependence of the event horizon radii of the Schwarzschild-like black hole (BH) on the spacetime parameters.

the event horizon as a function of the spacetime parameters in Fig. 2. It can be seen from this figure that the event horizon radii decrease under the influence of both the ξ and γ parameters.

Currently, we investigate the null geodesics around the Schwarzschild-like black hole (BH) in the presence of plasma by using the Hamilton-Jacobi equation. The Hamiltonian for the null geodesics around the BH in the presence of plasma can be expressed in the following form [25]:

$$\mathcal{H}(x^{\alpha}, p_{\alpha}) = \frac{1}{2}\left[g^{\alpha\beta}p_{\alpha}p_{\beta} - (n^2-1)(p_{\beta}u^{\beta})^2\right], \tag{3}$$

where x^{α}, u^{β}, and p_{α}, respectively, refer to the spacetime coordinate, four-velocity, and photon's momentum. Additionally, n represents the refractive index, and it can be defined as [66].

$$n^2 = 1 - \frac{\omega_p^2}{\omega^2}, \tag{4}$$

where ω_p and ω are the frequencies of the plasma and the photon, respectively. One can define them as

$$\omega_p^2(x^{\alpha}) = 4\pi e^2 N(x^{\alpha})/m_e, \ \omega(r) = \frac{\omega_0}{\sqrt{f(r)}}, \ \omega_0 = \text{const}, \tag{5}$$

with m_e, e, and N, respectively, representing electron mass, electron charge, and the number density of electrons. The metric function satisfies $f(r) \to 1$ as $r \to \infty$, while $\omega(\infty) = \omega_0 = -p_t$ defines the energy of a photon at spatial infinity. ω_0 can be restricted by using $\mathcal{H} = 0$ as

$$\frac{\omega_0^2}{f(r)} > \omega_p^2(r). \tag{6}$$

This condition physically implies that the photon's local frequency, $\omega(r)$, must exceed the plasma frequency at that location. Because this rule governs light in plasma, the resulting BH shadow can exhibit different forms than it does in the vacuum case ($\omega_p = 0$). Using Eq. (4), one can rewrite Eq. (3) as follows [25, 27].

$$\mathcal{H} = \frac{1}{2}\left[g^{\alpha\beta}p_{\alpha}p_{\beta} + \omega_p^2\right]. \tag{7}$$

Afterward, the light ray equations for the photon can be obtained by using $\dot{x}^{\alpha}=\partial\mathcal{H}/\partial p_{\alpha}$ in the equatorial plane $(\theta=\pi/2)$ as [67]

$$\dot{t}\equiv\frac{\mathrm{d}t}{\mathrm{d}\lambda}=-\frac{p_t}{f(r)}, \tag{8}$$

$$\dot{r}\equiv\frac{\mathrm{d}r}{\mathrm{d}\lambda}=p_r f(r), \tag{9}$$

$$\dot{\phi}\equiv\frac{\mathrm{d}\phi}{\mathrm{d}\lambda}=\frac{p_\phi}{r^2}. \tag{10}$$

We then derive the orbit equation by taking the ratio of Eqs. (9) and (10) as

$$\frac{\mathrm{d}r}{\mathrm{d}\phi}=\frac{g^{rr}p_r}{g^{\phi\phi}p_\phi}. \tag{11}$$

The equation above can be rewritten for the photon geodesics $\mathcal{H}=0$ in the following form [68]

$$\frac{\mathrm{d}r}{\mathrm{d}\phi}=\sqrt{\frac{g^{rr}}{g^{\phi\phi}}}\sqrt{h^2(r)\frac{\omega_0^2}{p_\phi^2}-1}, \tag{12}$$

with

$$h^2(r)\equiv-\frac{g^{tt}}{g^{\phi\phi}}-\frac{\omega_p^2}{g^{\phi\phi}\omega_0^2}. \tag{13}$$

When a light ray travels from infinity, reaches its closest approach at a radius $r_{\rm ps}$, and returns to infinity, this trajectory corresponds to a turning point in the $h^2(r)$ function. Consequently, the photon sphere radius is obtained by solving the equation below

$$\left.\frac{\mathrm{d}(h^2(r))}{\mathrm{d}r}\right|_{r=r_{\rm ps}}=0. \tag{14}$$

We numerically investigate the photon sphere radii due to the complex spacetime of the Schwarzschild-like BH. Figure 3 shows the photon sphere radii as a function of plasma frequency for different values of the ξ and γ parameters. As seen in this figure, the values of the radius of the photon sphere increase with the rise of the plasma frequency and vice versa for the ξ parameter. There is a slight decrease in the photon sphere radii under the influence of the γ parameter.

B. Black hole shadow in the presence of plasma

This subsection is devoted to the investigation of the BH shadow in plasma. One can write the angular radius of the shadow [24, 69]

$$\sin^2\alpha_{\rm sh}=\frac{h^2(r_{\rm ps})}{h^2(r_{\rm o})}=\frac{r_{\rm ps}^2\left[\dfrac{1}{f(r_{\rm ps})}-\dfrac{\omega_p^2(r_{\rm ps})}{\omega_0^2}\right]}{r_{\rm o}^2\left[\dfrac{1}{f(r_{\rm o})}-\dfrac{\omega_p^2(r_{\rm o})}{\omega_0^2}\right]}, \tag{15}$$

with $r_{\rm o}$ and $r_{\rm ps}$ referring to the locations of the observer and the photon sphere, respectively. We can approximate the BH shadow in the following form by assuming that the observer is located at a large distance from the BH [24]

$$R_{\rm sh}\simeq r_{\rm o}\sin\alpha_{\rm sh}=\sqrt{r_{\rm ps}^2\left[\frac{1}{f(r_{\rm ps})}-\frac{\omega_p^2(r_{\rm ps})}{\omega_0^2}\right]}. \tag{16}$$

1. *Homogeneous plasma*

In this section, we consider the homogeneous plasma distribution where the plasma frequency is constant, *i.e.*,

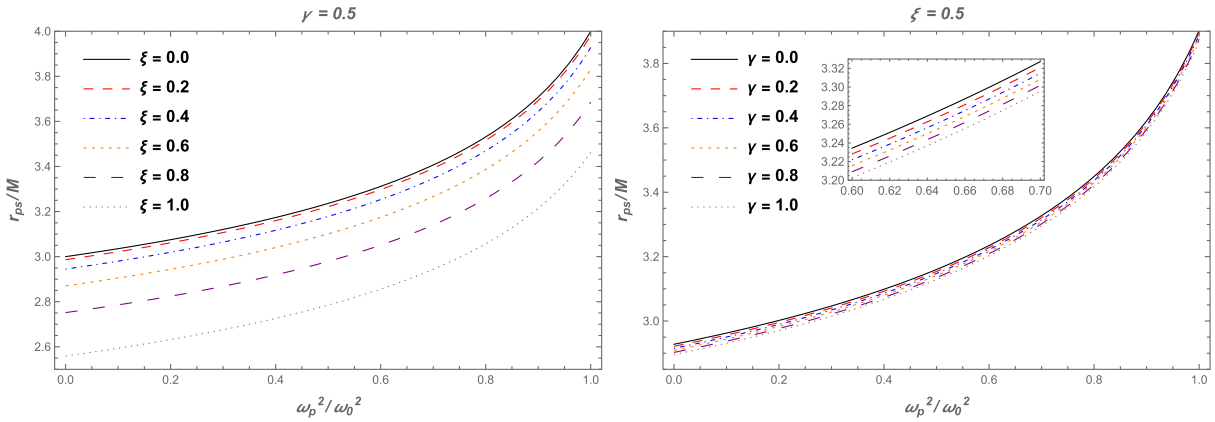

Fig. 3. (color online) The plot demonstrates the photon sphere radii as a function of the plasma frequency for different values of the ξ (left panel) and γ (right panel) parameters. Here, we set $\gamma=0.5$ for the left panel and $\xi=0.5$ for the right panel, respectively.

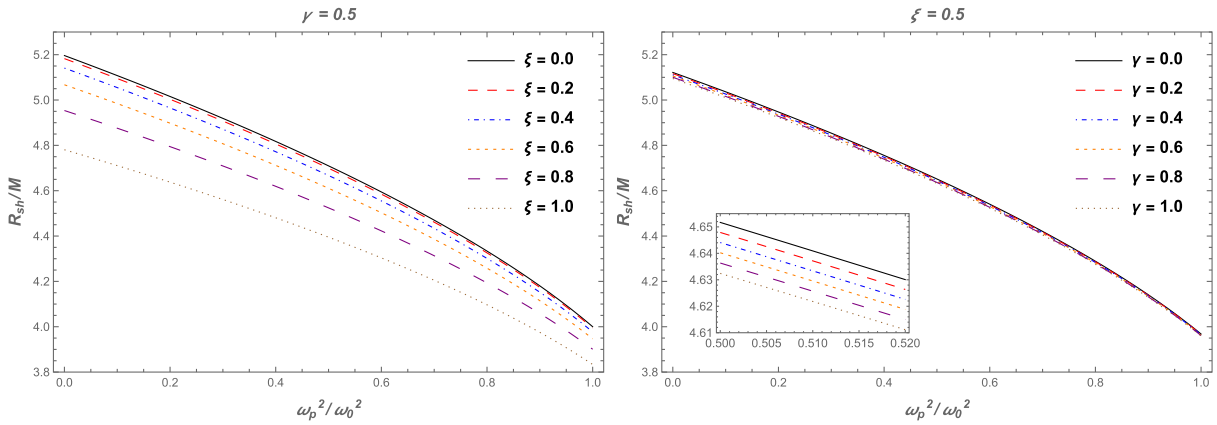

Fig. 4. (color online) The plot shows the dependence of the BH shadow radii on the plasma frequency for different values of the ξ (left panel) and γ (right panel) parameters. Here, we set $\gamma = 0.5$ and $\xi = 0.5$ for the left and right panels, respectively.

$\omega^2(r) = const$. In Fig. 4, we demonstrate the shadow radii as a function of the plasma frequency for different values of the ξ and γ parameters. It can be observed from this figure that the radius of the BH shadow decreases with an increase in both plasma frequency and the ξ parameter. There is also a slight decrease under the influence of the γ parameter. To provide more information, we explore the appearance of the BH shadow from the perspective of a distant observer. Therefore, we can write the following expressions using the celestial coordinates [69]

$$X = \lim_{r_0\to\infty}\left(-r_0\sin\theta_0\frac{\mathrm{d}\varphi}{\mathrm{d}r}\bigg|_{r_0,\theta_0}\right), \tag{17}$$

$$Y = \lim_{r_0\to\infty}\left(r_0\frac{\mathrm{d}\theta}{\mathrm{d}r}\bigg|_{r_0,\theta_0}\right), \tag{18}$$

where (r_0,θ_0) represents the position of the observer, the Eqs. (15) and (16) obey the following relation if we assume that the observer is located on the equatorial hyperplane

$$X^2 + Y^2 = R_{\rm sh}^2. \tag{19}$$

Using the above equation, we plot the BH shadow in Fig. 5. It can be seen from this figure that the BH shadow shrinks with the increase in the ξ parameter and the plasma frequency. Moreover, we obtain the theoretical constraints for the parameters of the spacetime and the plasma frequency by using the observational data from the EHT and GRAVITY collaborations, with the assumption that M87* and Sgr A* are static and spherically symmetric, despite the observations not supporting this. To do so, we can use the following equation to calculate the

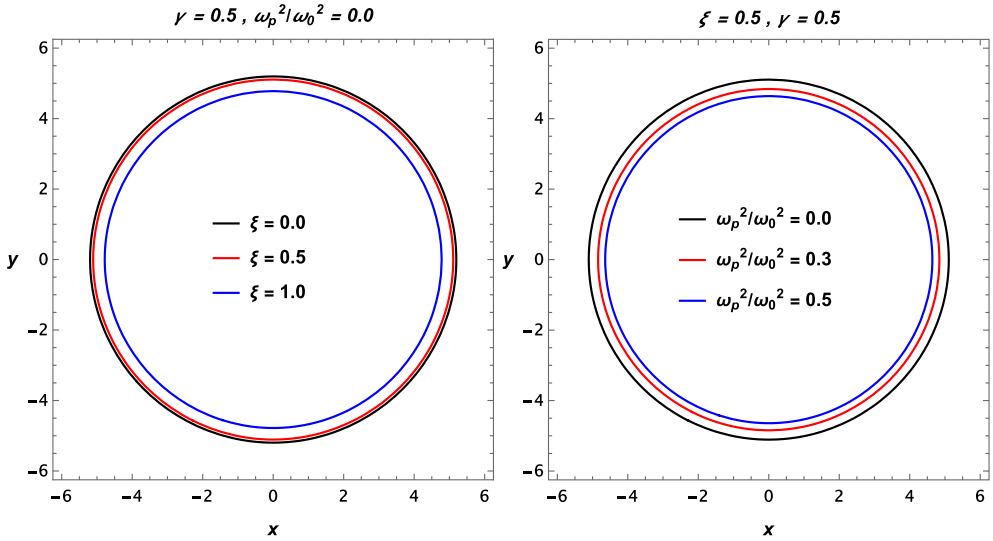

Fig. 5. (color online) The plot illustrates the profile of the shadow cast by the Schwarzschild-like black hole (BH) for different values of the ξ parameter and the plasma frequency.

Table 1. Observational data for M87* and Sgr A* are referenced in several studies [71–73].

Parameter	M87*	Sgr A*
Angular Diameter (θ)	$43.3 \pm 2.3\,\mu$as	$51.8 \pm 2.3\,\mu$as
Distance (D)	16.5 Mpc	8.275 kpc
Mass (M)	$(6.5 \pm 0.7) \times 10^9\, M_\odot$	$(4.297 \pm 0.013) \times 10^6\, M_\odot$

shadow diameter [70]

$$D_{\rm sh} = \frac{D\theta}{M}. \tag{20}$$

Using the observational data in Table 1, one can write the diameter of the shadow as follows:

$$\begin{aligned} D_{\rm sh}^{\rm M87^*} &= (11 \pm 1.5)M, \\ D_{\rm sh}^{\rm Sgr\ A^*} &= (9.5 \pm 1.4)M. \end{aligned} \tag{21}$$

Using the simple equation $D_{\rm sh} = 2R_{\rm sh}$, one can constrain the values of the spacetime parameters and the plasma frequency. These results were demonstrated in the top panel (for M87*) and the bottom panel (for Sgr A*) of Fig. 6. Indeed, the typical electron densities near the event horizons of M87* and Sgr A* are estimated at $10^4 - 10^5$ cm^{-3} and $10^6 - 10^8$ cm^{-3}, respectively. While a simple calculation yields a ratio of $(\omega_p/\omega)^2 \approx 10^{-7}$ at 230 GHz for these average densities, we emphasize that plasma effects remain non-trivial due to the fact that global averages may overlook localized regions of significantly higher density ($10^{10} - 10^{12}$ cm^{-3}) within the turbulent accretion flow or at the base of the jet, where $(\omega_p/\omega)^2$ is large enough to affect the shadow of the black hole.

2. *Inhomogeneous plasma*

Here, we investigate the BH shadow by assuming that the BH is surrounded by inhomogeneous plasma. The plasma frequency can be expressed in a simple power-

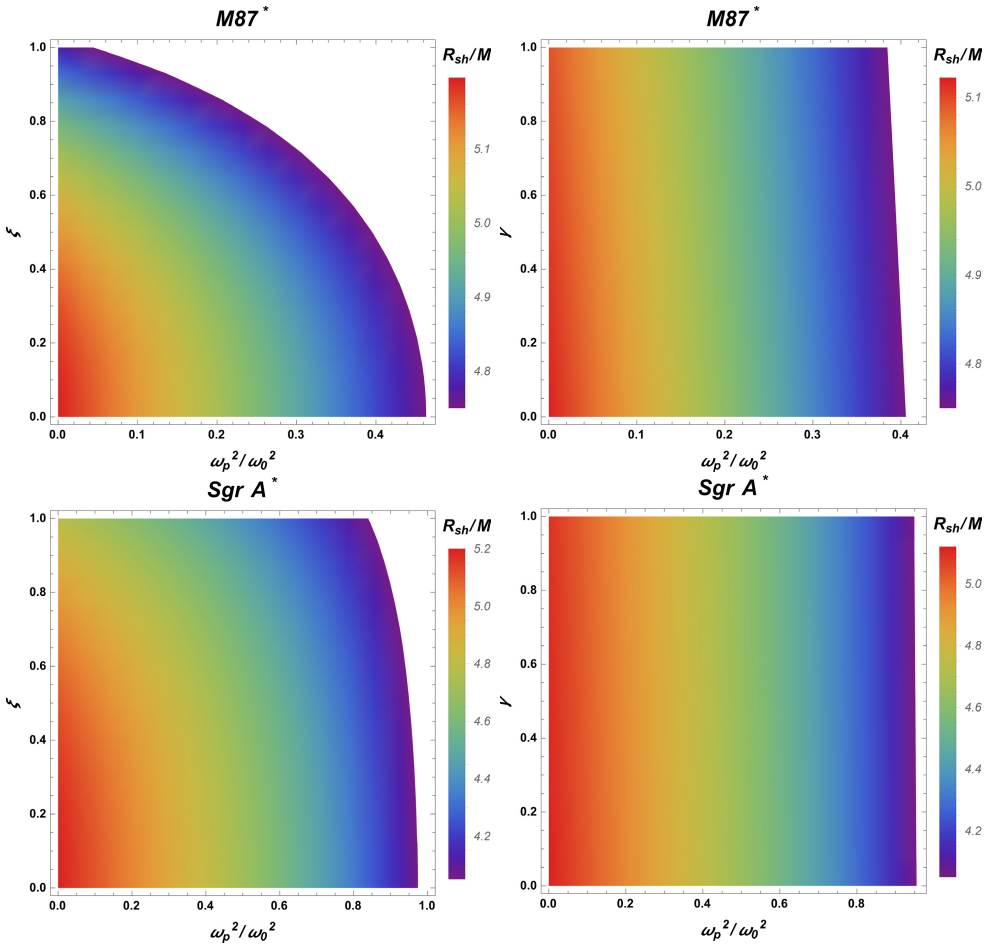

Fig. 6. (color online) The plot illustrates the radius of the black hole (BH) shadow for M87* (top panels) and Sgr A* (bottom panels) as a function of the spacetime parameters and the plasma frequency. The values of the shadow radius are derived from Eq. (21). In this context, we set $\gamma = 0.5$ for the left panels and $\xi = 0.5$ for the right panels.

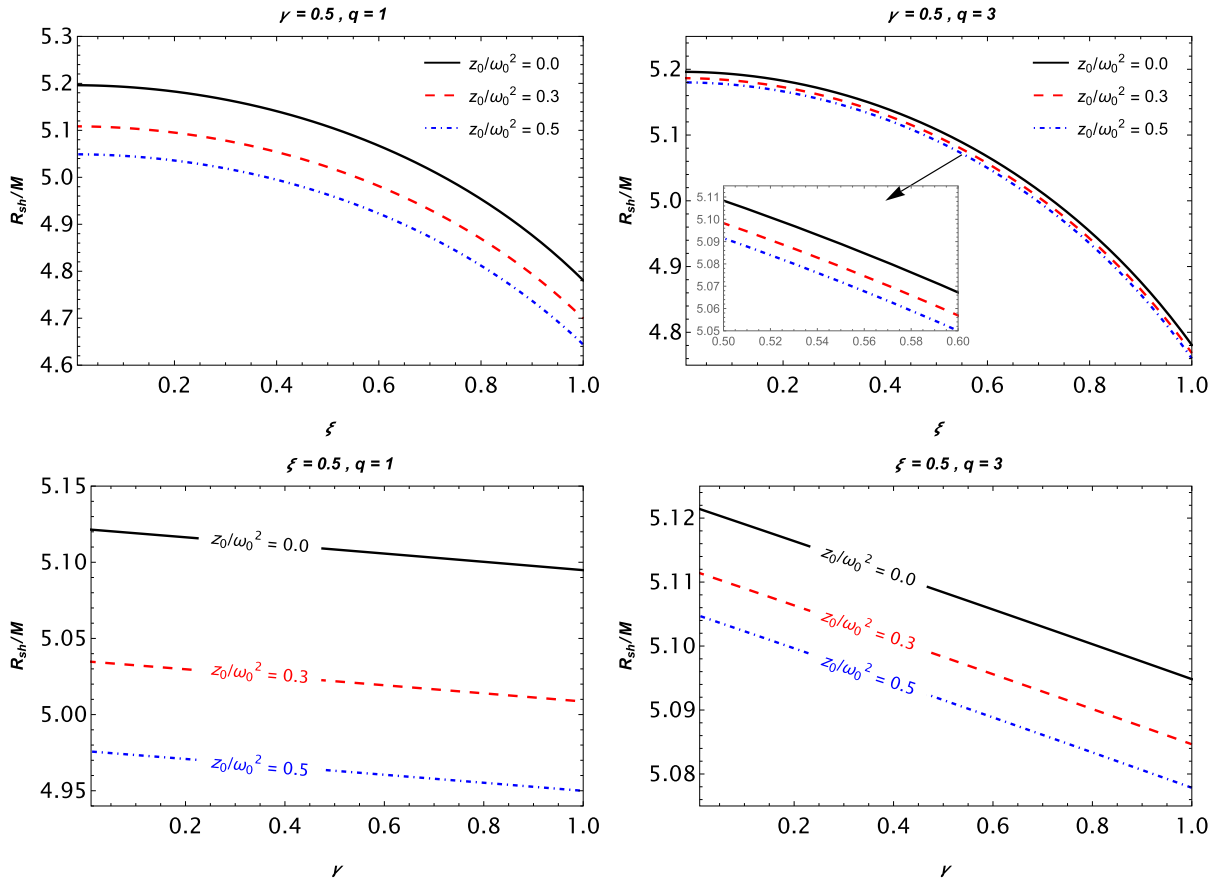

Fig. 7. (color online) The top panel illustrates the BH shadow radius as a function of the ξ parameter for various values of z_0/ω_0^2. In the bottom panel, the plot reveals the dependence of the shadow radius on the γ parameter for different values of z_0/ω_0^2. Here, we set $q=1$ and $q=3$ for the left and right panels, respectively, while $\gamma=0.5$ and $\xi=0.5$ are used for the top and bottom panels.

law form as follows [74, 75]

$$\omega_p^2(r)=\frac{z_0}{r^q}, \tag{22}$$

where z_0 and $q>0$ are considered free parameters. To investigate the fundamental characteristics of the aforementioned model, we consider the following two particular scenarios:

- When $q=1$ and z_0 remains constant, this corresponds precisely to the negative-mass diverging lens model.

- The case of $q=3$ with fixed z_0 refers to a profile associated with the stellar surface based on the Goldreich-Julian density [76].

Now, in Fig. 7, we plot the radius of the BH shadow as a function of the spacetime parameters for different values of z_0, using the values of q as specified earlier. This figure shows that the shadow radii decrease as z_0/ω_0^2 increases, and there is a slight difference between the $q=1$ and $q=3$ cases. To provide more information, we plot the BH shadow in the presence of the inhomogeneous plasma in Fig. 8. In addition to the effect of the spacetime parameters, we can observe a slight decrease with the increase in z_0/ω_0^2. Moreover, we compare the impact of the homogeneous and inhomogeneous plasma on the radius of the BH shadow in Fig. 9. As can be seen from this figure, the homogeneous plasma has a stronger effect on decreasing the shadow radii than the inhomogeneous case.

III. WEAK GRAVITATIONAL LENSING FOR BLACK HOLE

This section focuses on the framework of gravitational weak lensing around Schwarzschild-like black holes in the presence of both uniform and non-uniform plasma cases. To proceed, we need to define the weak-field approximation as outlined in [20, 68]

$$g_{\alpha\beta}=\eta_{\alpha\beta}+h_{\alpha\beta}. \tag{23}$$

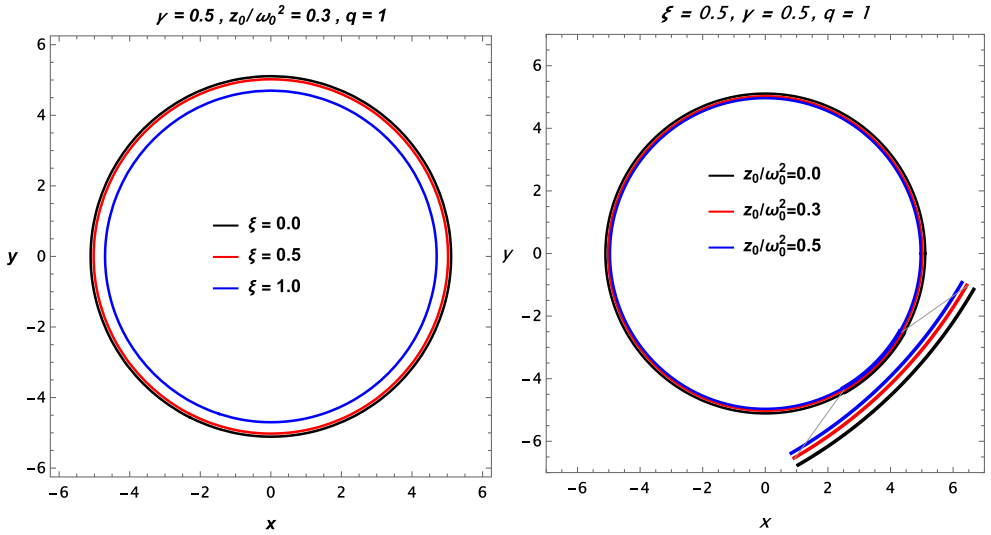

Fig. 8. (color online) The plot illustrates the profile of the shadow cast by the Schwarzschild-like black hole for different values of the ξ parameter and the z_0/ω_0^2 ratio.

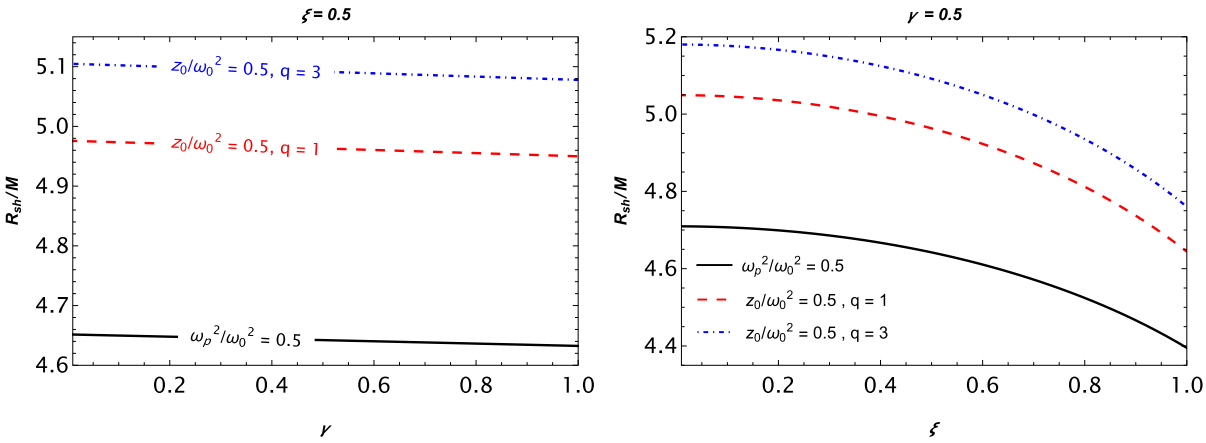

Fig. 9. (color online) The plot compares the effects of homogeneous and inhomogeneous plasma on the radius of the BH shadow for the given values of the spacetime and plasma parameters.

Here, $\eta_{\alpha\beta}$ and $h_{\alpha\beta}$ represent the Minkowski spacetime and the gravitational perturbation, respectively. Therefore, the following conditions are suitable for them:

$$\begin{aligned} &\eta_{\alpha\beta} = \mathrm{diag}(-1,1,1,1)\,, \\ &h_{\alpha\beta} \ll 1, \quad h_{\alpha\beta} \to 0 \quad \text{under} \quad x^{\alpha} \to \infty\,, \\ &g^{\alpha\beta} = \eta^{\alpha\beta} - h^{\alpha\beta}, \quad h^{\alpha\beta} = h_{\alpha\beta}\,. \end{aligned} \tag{24}$$

One can use the following equation to investigate the deflection angle around the BH [20].

$$\hat{\alpha}_b = \frac{1}{2}\int_{-\infty}^{\infty}\frac{b}{r}\left(\frac{\mathrm{d}h_{33}}{\mathrm{d}r} + \frac{1}{1-\omega_p^2/\omega^2}\frac{\mathrm{d}h_{00}}{\mathrm{d}r} - \frac{K_e}{\omega^2-\omega_p^2}\frac{\mathrm{d}N}{\mathrm{d}r}\right)\mathrm{d}z, \tag{25}$$

with ω and ω_p respectively referring to the frequencies of the photon and plasma. Here, b represents the impact parameter, signifying the closest approach of the photons to the BH, and K_e is a constant defined by $K_e = 4\pi e^2/m$ [20]. To explore weak gravitational lensing, we need to expand the line element of the Schwarzschild-like BH into a Taylor series in the following form:

$$\begin{aligned} \mathrm{d}s^2 \approx \mathrm{d}s_0^2 &+ \frac{4Mr^2}{\xi^2(\gamma M + r) + \sqrt{\xi^4(\gamma M + r)^2 + 4r^6}}\mathrm{d}t^2 \\ &+ \frac{4Mr^2}{\xi^2(\gamma M + r) + \sqrt{\xi^4(\gamma M + r)^2 + 4r^6}}\mathrm{d}r^2\,. \end{aligned} \tag{26}$$

where $\mathrm{d}s_0^2 = -\mathrm{d}t^2 + \mathrm{d}r^2 + r^2(\mathrm{d}\theta^2 + \sin^2\theta\,\mathrm{d}\phi^2)$. We further write the components of $h_{\alpha\beta}$ as

$$h_{00} = \frac{4Mr^2}{\xi^2(\gamma M + r) + \sqrt{\xi^4(\gamma M + r)^2 + 4r^6}},$$
$$h_{ik} = \frac{4Mr^2}{\xi^2(\gamma M + r) + \sqrt{\xi^4(\gamma M + r)^2 + 4r^6}} n_i n_k,$$
$$h_{33} = \frac{4Mr^2}{\xi^2(\gamma M + r) + \sqrt{\xi^4(\gamma M + r)^2 + 4r^6}} \cos^2\chi, \quad (27)$$

where we define z as the coordinate along the photon trajectory. For a light ray with impact parameter b, the radial distance r is related to z via $r^2 = b^2 + z^2$, and χ represents the angle between the radial vector and the direction of propagation, such that $\cos^2\chi = z^2/r^2$. After that, it is possible to write the deflection angle as a combination of three angles as follows [77]

$$\hat{\alpha}_b = \hat{\alpha}_1 + \hat{\alpha}_2 + \hat{\alpha}_3, \quad (28)$$

with

$$\hat{\alpha}_1 = \frac{1}{2}\int_{-\infty}^{\infty} \frac{b}{r}\frac{\mathrm{d}h_{33}}{\mathrm{d}r}\mathrm{d}z,$$
$$\hat{\alpha}_2 = \frac{1}{2}\int_{-\infty}^{\infty} \frac{b}{r}\frac{1}{1-\omega_p^2/\omega^2}\frac{\mathrm{d}h_{00}}{\mathrm{d}r}\mathrm{d}z,$$
$$\hat{\alpha}_3 = \frac{1}{2}\int_{-\infty}^{\infty} \frac{b}{r}\left(-\frac{K_e}{\omega^2-\omega_p^2}\frac{\mathrm{d}N}{\mathrm{d}r}\right)\mathrm{d}z. \quad (29)$$

In the subsequent sections, we investigate the deflection angle in the presence of both uniform and non-uniform plasma density distributions.

A. Uniform plasma

The equation (28) can be written for the uniform plasma case as [77, 78]

$$\hat{\alpha}_{\rm uni} = \hat{\alpha}_{\rm uni1} + \hat{\alpha}_{\rm uni2} + \hat{\alpha}_{\rm uni3}. \quad (30)$$

We can analyze the deflection angle numerically by combining Eqs. (27), (28), and (29). The left panel of Fig. 10 demonstrates the deflection angle as a function of the impact parameter for different values of the plasma frequency. As shown in this figure, the values of the deflection angle decrease with the rise of the impact parameter, and vice versa, for the uniform plasma frequency. Here, we set the spacetime parameters as $\xi = \gamma = 0.5$. We plot the dependence of $\hat{\alpha}_{\rm uni}$ on the ξ parameter for different values of the γ parameter in the right panel of Fig. 10. One can observe from this panel that the deflection angle decreases with increasing values of both ξ and γ.

B. Non uniform plasma

In this subsection, we examine the singular isothermal sphere (SIS), which is the most widely favored model for probing photon geodesics near black holes (BHs). Typically described as a spherical gas cloud, it features a central singularity where density becomes theoretically infinite. The SIS density distribution can be written as follows [20]

$$\rho(r) = \frac{\sigma_v^2}{2\pi r^2}, \quad (31)$$

with σ_v^2 is referring an one-dimensional velocity dispersion. Subsequently, we can write the plasma frequency in the following form

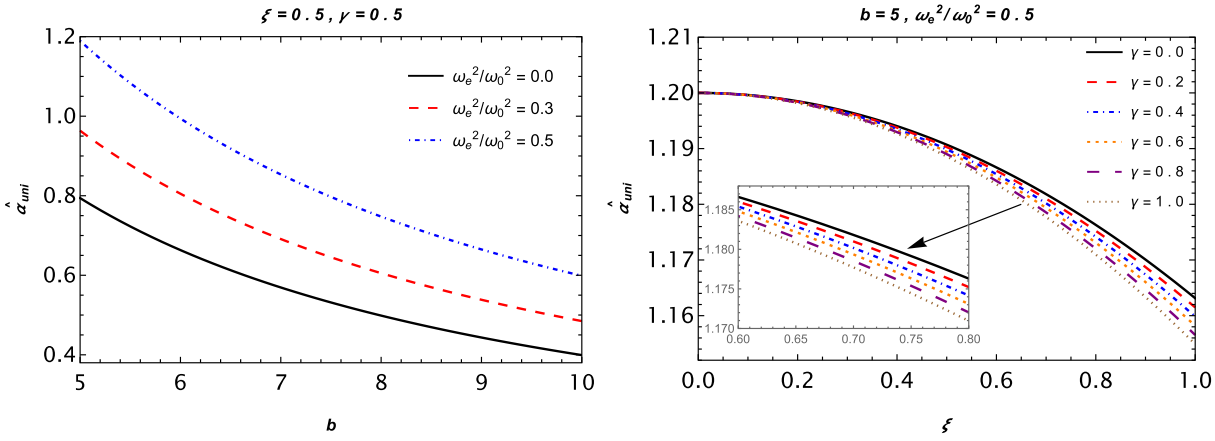

Fig. 10. (color online) The left panel shows the deflection angle as a function of the impact parameter for different values of the uniform plasma frequency. Here, we set the spacetime parameters as $\xi = 0.5$ and $\gamma = 0.5$. The right panel illustrates the dependence of the deflection angle on the ξ parameter for different values of the γ parameter. The impact parameter and the plasma frequency were fixed for this panel, *i.e.*, $b = 5$ and $\omega_e^2/\omega_0^2 = 0.5$.

$$\omega_c^2 = K_e N(r) = \frac{K_e \sigma_v^2}{2\pi k m_p r^2}. \tag{32}$$

Keeping this in mind, the deflection angle for the non-uniform plasma case can be written by combining three angles as

$$\hat{\alpha}_{\rm SIS} = \hat{\alpha}_{\rm SIS1} + \hat{\alpha}_{\rm SIS2} + \hat{\alpha}_{\rm SIS3}. \tag{33}$$

We plot the dependence of the deflection angle in the presence of the non-uniform plasma on the impact parameter for the different values of the plasma frequency in the left panel of Fig. 11. It can be seen from this panel that there is a decrease with the increase in the values of the impact parameter and plasma frequency. Furthermore, the deflection angle for the non-uniform plasma was plotted as a function of the ξ parameter for the different values of the γ parameter. As shown in this panel, there is a slight decrease under the influence of both ξ and γ parameters. It should be noted that the effects of uniform and non-uniform plasma cases on the deflection angle are opposite to each other. We compare the deflection angle of light for the uniform and non-uniform plasma cases in Fig. 12 to provide more information.

IV. MAGNIFICATION OF GRAVITATIONALLY LENSED IMAGE

This section is devoted to the magnification of the gravitationally lensed image around the Schwarzschild-like BH surrounded by uniform and non-uniform plasma. One can define the magnification factors in the presence of the plasma, which are $\mu_+^{\rm pl}$ and $\mu_-^{\rm pl}$, referring to the primary and secondary images, respectively, as [32, 34, 79, 80].

$$\mu_+^{\rm pl} = \frac{1}{4}\left(\frac{x}{\sqrt{x^2+4}} + \frac{\sqrt{x^2+4}}{x} + 2\right), \tag{34}$$

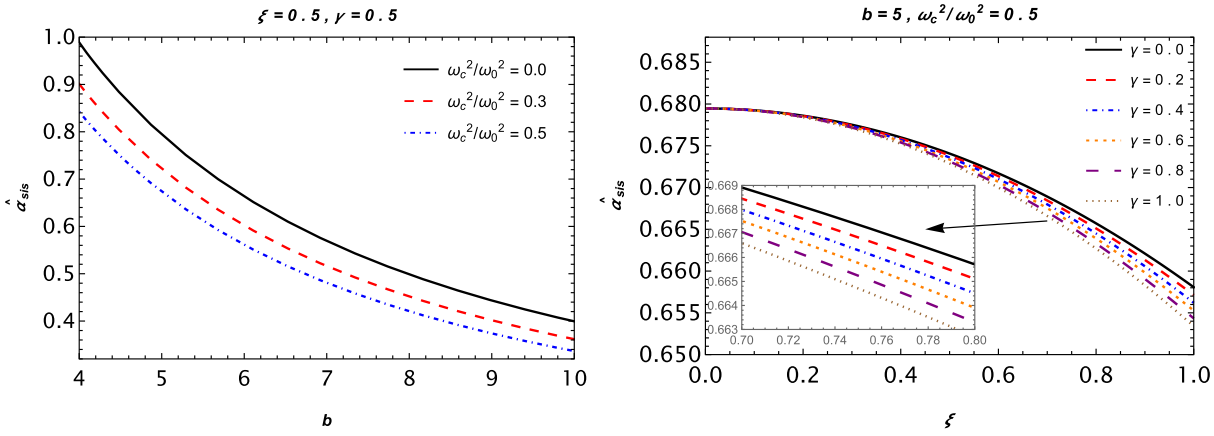

Fig. 11. (color online) The same as Fig. 10, but for the non-uniform plasma scenario.

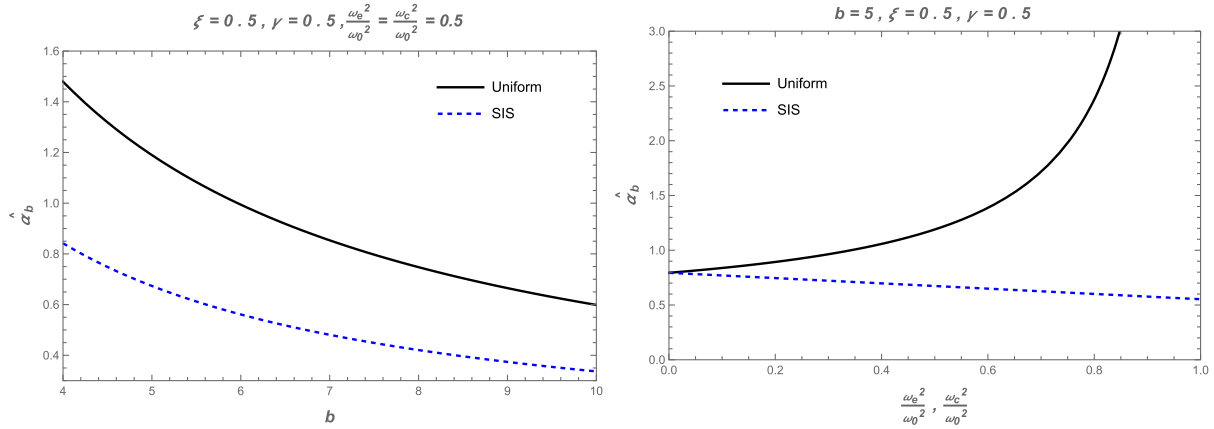

Fig. 12. (color online) Illustrated in the plot is a comparison of the deflection angle between uniform and non-uniform plasma distributions. The dependence on the impact parameter is shown in the left panel, and the dependence on the plasma frequency is shown in the right panel.

$$\mu_{-}^{\rm pl}=\frac{1}{4}\left(\frac{x}{\sqrt{x^2+4}}+\frac{\sqrt{x^2+4}}{x}-2\right), \tag{35}$$

where [68]

$$x=\beta/\theta_{\rm E}, \tag{36}$$

with $\theta_{\rm E}$ referring to Einstein's ring, which defines the shape of the image, and β referring to the angular position of the source with respect to the line passing through the observer and the lens, one can then calculate the total magnification as a combination of the magnification factors as [78].

$$\mu_{\rm tot}^{\rm pl}=\mu_{+}^{\rm pl}+\mu_{-}^{\rm pl}=\frac{x^2+2}{x\sqrt{x^2+4}}. \tag{37}$$

In the next subsections, we analyze the effect of both uniform and non-uniform plasma on the total magnification.

A. Uniform plasma

In this section, we consider a uniform plasma. Therefore, Eq. (37) can be rewritten as follows:

$$\left(\mu_{\rm tot}^{\rm pl}\right)_{\rm uni}=\left(\mu_{+}^{\rm pl}\right)_{\rm uni}+\left(\mu_{-}^{\rm pl}\right)_{\rm uni}=\frac{x_{\rm uni}^2+2}{x_{\rm uni}\sqrt{x_{\rm uni}^2+4}}, \tag{38}$$

where

$$\begin{aligned}(\mu_{\pm}^{\rm pl})_{\rm uni}&=\frac{1}{4}\left(\frac{x_{\rm uni}}{\sqrt{x_{\rm uni}^2+4}}+\frac{\sqrt{x_{\rm uni}^2+4}}{x_{\rm uni}}\pm 2\right),\\ x_{\rm uni}&=\frac{\beta}{(\theta_{\rm E}^{\rm pl})_{\rm uni}}.\end{aligned} \tag{39}$$

We plot the total magnification as a function of the uniform plasma frequency for different values of the ξ para-

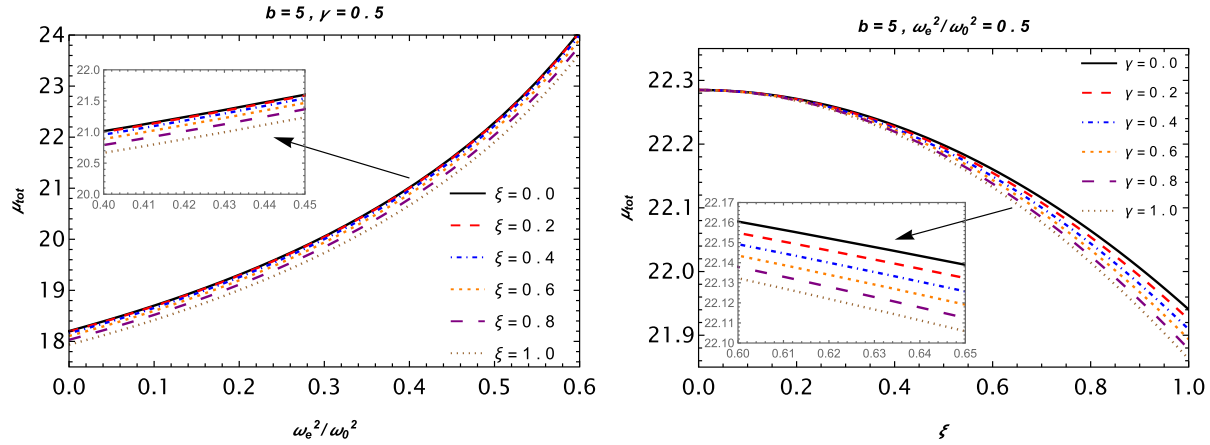

Fig. 13. (color online) Left panel: The total magnification as a function of the uniform plasma frequency for different values of the ξ parameter, with other parameters fixed at $b=5$ and $\gamma=0.5$. The right panel shows the dependence of the total magnification on the ξ parameter for different values of the γ parameter. Here, we set $b=5$ and $\omega_e^2/\omega_0^2=0.5$.

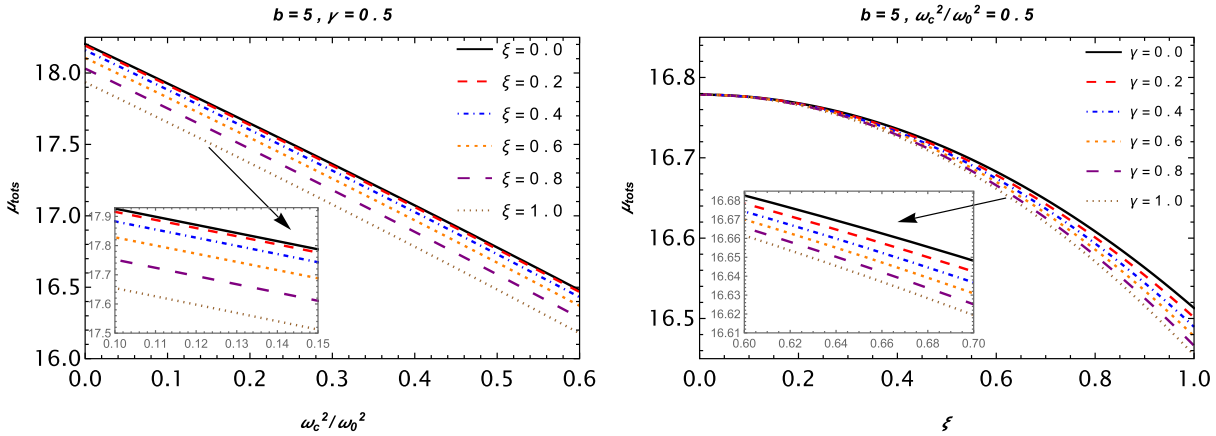

Fig. 14. (color online) The same as Fig. 13, but for the non-uniform plasma scenario.

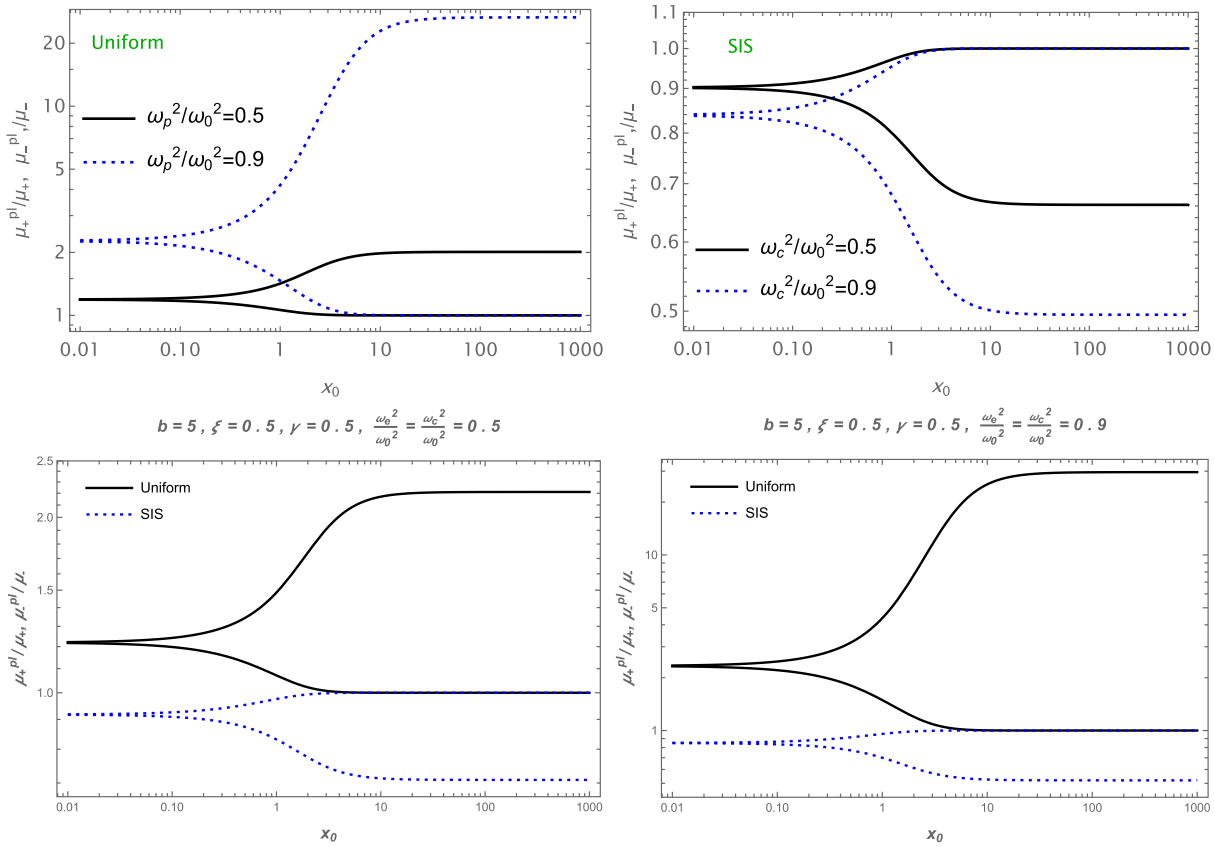

Fig. 15. (color online) The top left and right panels illustrate the ratio of the magnification factors in the presence of plasma to those in the vacuum case as a function of x_0 for different values of the plasma frequencies, while their comparisons are presented in the bottom panels.

meter while the other parameters are fixed as $b=5$, $\gamma=0.5$ in the left panel of Fig. 13. One can see from this panel that the total magnification increases with the rise in the uniform plasma frequency. Also, there is a slight decrease influenced by the ξ parameter. In the right panel of this figure, the dependence of the total magnification on the ξ parameter for different values of the γ parameter is plotted. It is clear from this panel that the total magnification decreases due to the rise of the spacetime parameters. Here, the other parameters are considered constant, as $b=5$ and $\omega_e^2/\omega_0^2=0.5$.

B. Non-uniform plasma

As conducted in the previous section, we examine the effect of the non-uniform plasma on the total magnification. Hence, we recall Eq. (37) for the non-uniform plasma (SIS medium) as in [20].

$$\left(\mu_{\rm tot}^{\rm pl}\right)_{\rm SIS}=\left(\mu_{+}^{\rm pl}\right)_{\rm SIS}+\left(\mu_{-}^{\rm pl}\right)_{\rm SIS}=\frac{x_{\rm SIS}^2+2}{x_{\rm SIS}\sqrt{x_{\rm SIS}^2+4}}, \tag{40}$$

with

$$(\mu_{\pm}^{\rm pl})_{\rm SIS}=\frac{1}{4}\left(\frac{x_{\rm SIS}}{\sqrt{x_{\rm SIS}^2+4}}+\frac{\sqrt{x_{\rm SIS}^2+4}}{x_{\rm SIS}}\pm 2\right),$$
$$x_{\rm SIS}=\frac{\beta}{(\theta_{\rm E}^{\rm pl})_{\rm SIS}}. \tag{41}$$

Using the above equations, we plot the dependence of the total magnification on the non-uniform plasma frequency for different values of the ξ parameter in the left panel of Fig. 14. We can see from this panel that the total magnification decreases under the influence of both the plasma frequency and the ξ parameter. Furthermore, the total magnification as a function of the ξ parameter was plotted for different values of the γ parameter in the right panel of Fig. 14. It can be seen from this panel that there is a slight decrease with the increase in the spacetime parameters. Additionally, we plot the ratio of the magnification factors to that of the vacuum case as a function of x_0 for both the uniform and non-uniform plasma cases, alongside a comparison between these cases in Fig. 15. Notably, this ratio increases with an increase in the plasma frequency in the uniform plasma case and decreases in the non-uniform plasma case. Also, the uni-

form plasma distribution exhibits greater sensitivity to this ratio compared to the non-uniform one.

V. CONCLUSIONS

In this work, we analyze the impact of uniform and non-uniform plasma on the shadow and weak gravitational lensing around the Schwarzschild-like BH. Our key results from the research can be summarized as follows:

First, we perform an analysis of the spacetime geometry by plotting the radial dependence of the metric function for different values of the ξ and γ parameters. We then investigate the event horizon structure of the Schwarzschild-like BH. It was found that the event horizon radii decrease as both spacetime parameters increase. In addition, using the Hamiltonian formalism, we study the photon dynamics around the BH in the presence of homogeneous plasma together with the BH shadow. The outcomes indicate that the photon sphere radii increase under the influence of the plasma frequency, while the BH shadow radii decrease. Also, both decrease with the rise of the ξ and γ parameters. After that, we constrain the spacetime parameters and the homogeneous plasma frequency using the observational data for M87* and Sgr A*.

Moreover, we investigate another observational signature of the Schwarzschild-like BH, which is weak gravitational lensing in the presence of uniform and non-uniform plasma. We explore the deflection angle for both cases numerically due to the complexity of the considered spacetime, and we find that the deflection angle increases with the increase of the uniform plasma frequency, while it decreases for the non-uniform case. The rise in the spacetime parameters leads to a reduction in the deflection angle values for both cases.

Finally, we study the magnification of the gravitationally lensed image. Using Einstein's ring, we define the magnification factors for the primary and secondary images and find the total magnification by linearly combining them. Subsequently, we plot the total magnification for the uniform and non-uniform cases as a function of the plasma frequency and the ξ parameter. The results indicate a decrease with the increase of the ξ and γ parameters, and the total magnification decreases under the influence of the non-uniform plasma frequency, while for the uniform case, it is vice versa. To elaborate further, we plot the ratio of the magnification factors in the presence of plasma to those in the vacuum case. Notably, the values of this ratio increase/decrease under the influence of the uniform/non-uniform plasma frequency.

Investigating the optical phenomena around BHs, including the Schwarzschild-like BH, is crucial from an astrophysical perspective. Our theoretical findings may not advance fundamental understanding but could open a window for future observational and experimental efforts to distinguish Schwarzschild-like BHs from ordinary Schwarzschild BHs.

ACKNOWLEDGEMENT

We warmly thank the anonymous referees for their valuable comments and discussions that helped to improve the accuracy and quality of the manuscript's presentation.

References

[1] K. Akiyama *et al*. (Event Horizon Telescope Collaboration), Astrophys. J. Lett. **875**, L1 (2019), arXiv: 1906.11238 [astro-ph.GA]
[2] K. Akiyama *et al*. (Event Horizon Telescope Collaboration), Astrophys. J. Lett. **875**, L4 (2019), arXiv: 1906.11241 [astro-ph.GA]
[3] K. Akiyama *et al*. (Event Horizon Telescope Collaboration), Astrophys. J. Lett. **930**, L12 (2022), arXiv: 2311.08680 [astro-ph.HE]
[4] B. P. Abbott and others (LIGO Scientific Collaboration and Virgo Collaboration), Phys. Rev. Lett. **116**, 061102 (2016), arXiv: 1602.03837[gr-qc]
[5] A. Duran-Cabacxes, D. Rubiera-Garcia, and D. SxaezChillxon Gxomez, Phys. Rev. D **112**, 044016 (2025), arXiv: 2506.10814[gr-qc]
[6] M. Guerrero, G. J. Olmo, D. Rubiera-Garcia *et al*., JCAP (08), 036 (2021), arXiv: 2105.15073[grqc]
[7] G. J. Olmo, J. L. Rosa, D. Rubiera-Garcia *et al*., Class. Quant. Grav. **40**, 174002 (2023), arXiv: 2302.12064[gr-qc]
[8] S. E. Gralla, D. E. Holz, and R. M. Wald, Phys. Rev. D **100**, 024018 (2019), arXiv: 1906.00873[astroph.HE]
[9] R. Penrose, Phys. Rev. Lett. **14**, 57 (1965)
[10] M. Reuter, Phys. Rev. D **57**, 971 (1998), arXiv: hepth/9605030
[11] M. Niedermaier and M. Reuter, Living Reviews in Relativity **9**, 5 (2006)
[12] M. Reuter and F. Saueressig, *Quantum Gravity and the Functional Renormalization Group: The Road towards Asymptotic Safety*, (Cambridge University Press, 2019)
[13] A. Bonanno and M. Reuter, Phys. Rev. D **62**, 043008 (2000), arXiv: hep-th/0002196
[14] A. Bonanno and M. Reuter, Phys. Rev. D **73**, 083005 (2006), arXiv: hep-th/0602159
[15] K. Falls, C. R. King, D. F. Litim *et al*., Phys. Rev. D **97**, 086006 (2018), arXiv: 1801.00162[hep-th]
[16] G. Alencar, T. M. Crispim, C. R. Muniz *et al*., (2026), arXiv: 2603.05130v1[gr-qc]
[17] J. L. Synge, *Relativity: The General Theory* (NorthHolland, Amsterdam, 1960)
[18] V. Perlick, Living Reviews in Relativity **7**, 9 (2004)
[19] O. Y. Tsupko and G. S. Bisnovatyi-Kogan, MNRAS **427**, 2017 (2012)
[20] G. S. Bisnovatyi-Kogan and O. Y. Tsupko, MNRAS **404**, 1790 (2010), arXiv: 1006.2321[astro-ph.CO]
[21] F. Feleppa, V. Bozza, and O. Y. Tsupko, Phys. Rev. D **110**,

064031 (2024)
[22] F. Feleppa, V. Bozza, and O. Y. Tsupko, Phys. Rev. D **111**, 044018 (2025)
[23] F. Feleppa, F. Aratore, and V. Bozza, Phys. Rev. D **112**, 1 (2025)
[24] V. Perlick, O. Y. Tsupko, and G. S. Bisnovatyi-Kogan, Phys. Rev. D **92**, 104031 (2015)
[25] J. L. Synge, MNRAS**131**, 463 (1966)
[26] V. Bozza, Phys. Rev. D **66**, 103001 (2002), arXiv: gr-qc/0208075
[27] A. Rogers, MNRAS **451**, 17 (2015)
[28] V. S. Morozova, B. J. Ahmedov, and A. A. Tursunov, Astrophys. Space Sci. **346**, 513 (2013)
[29] A. Abdujabbarov, B. Toshmatov, Z. Stuchlxık *et al.*, Int. J. Mod. Phys. D **25**, 1650023 (2015)
[30] M. Alloqulov, S. Shaymatov, A. Jawad *et al.*, Commun. Theor. Phys. **77**, 015402 (2025)
[31] A. Al-Badawi, M. Alloqulov, S. Shaymatov *et al.*, Chin. Phys. C **48**, 095105 (2024)
[32] M. Alloqulov, F. Atamurotov, A. Abdujabbarov *et al.*, Chin. Phys. C **47**, 075103 (2023)
[33] H. Jiang, M. Alloqulov, Q. Wu *et al.*, Phys. Dark Univ. **46**, 101627 (2024)
[34] M. Alloqulov, F. Atamurotov, A. Abdujabbarov *et al.*, Chin. Phys. C **48**, 115116 (2024)
[35] A. Al-Badawi, S. Shaymatov, M. Alloqulov *et al.*, Commun. Theor. Phys. **76**, 085401 (2024)
[36] M. Alloqulov, F. Atamurotov, A. Abdujabbarov *et al.*, Chin. Phys. C **48**, 025104 (2024)
[37] F. Atamurotov, M. Alloqulov, A. Abdujabbarov *et al.*, Eur. Phys. J. Plus **137**, 634 (2022)
[38] J. Sharipov, M. Alloqulov, P. Sheoran *et al.*, Chin. J Phys. **99**, 461 (2026)
[39] M. Alloqulov, Y. Isaqjonov, S. Shaymatov *et al.*, Chin. Phys. C **49**, 045104 (2025)
[40] J. Khasanov, M. Alloqulov, P. Sheoran *et al.*, JCAP **12**, 023 (2025)
[41] W. Javed, I. Hussain, and A. Övgün, Eur. Phys. J. Plus **137**, 148 (2022), arXiv: 2201.09879[gr-qc]
[42] F. Atamurotov, I. Hussain, G. Mustafa *et al.*, Chin. Phys. C **47**, 025102 (2023)
[43] B. Turimov, O. Rahimov, A. Davlataliev *et al.*, Phys. Dark Univ. **48**, 101855 (2025), arXiv: 2502.11210[gr-qc]
[44] A. Davlataliev, B. Narzilloev, I. Hussain *et al.*, Phys. Dark Univ. **42**, 101340 (2023)
[45] A. Chowdhuri and A. Bhattacharyya, Phys. Rev. D **104**, 064039 (2021)
[46] E. Battista, S. Capozziello, and C. Y. Chen, (2026), arXiv: 2601.10806[gr-qc]
[47] K. S. Virbhadra, Phys. Rev. D **109**, 124004 (2024), arXiv: 2402.17190[gr-qc]
[48] K. S. Virbhadra, Can. J. Phys. **102**, 523 (2024), arXiv: 2204.01792[gr-qc]
[49] S. L. Adler and K. S. Virbhadra, Gen. Rel. Grav. **54**, 93 (2022), arXiv: 2205.04628[gr-qc]
[50] K. S. Virbhadra, Phys. Rev. D **106**, 064038 (2022), arXiv: 2204.01879[gr-qc]
[51] K. S. Virbhadra and C. R. Keeton, Phys. Rev. D **77**, 124014 (2008), arXiv: 0710.2333[gr-qc]
[52] K. S. Virbhadra, Phys. Rev. D **79**, 083004 (2009), arXiv: 0810.2109[gr-qc]
[53] K. S. Virbhadra, D. Narasimha, and S. M. Chitre, Astron. Astrophys. **337**, 1 (1998), arXiv: astro-ph/9801174
[54] C. M. Claudel, K. S. Virbhadra, and G. F. R. Ellis, J. Math. Phys. **42**, 818 (2001), arXiv: gr-qc/0005050
[55] K. S. Virbhadra and G. F. R. Ellis, Phys. Rev. D **65**, 103004 (2002)
[56] K. S. Virbhadra and G. F. R. Ellis, Phys. Rev. D **62**, 084003 (2000), arXiv: astro-ph/9904193
[57] Y. Mizuno, Z. Younsi, C. M. Fromm *et al.*, Nature Astron. **2**, 585 (2018), arXiv: 1804.05812[astro-ph.GA]
[58] M. Zhang, Y. Mizuno, C. M. Fromm *et al.*, Astron. Astrophys. **687**, A88 (2024), arXiv: 2404.04033[astro-ph.HE]
[59] Y. Song, Y. Hou, L. Huang, and B. Chen, Phys. Rev. D **113**, 043054 (2026), arXiv: 2507.23281[astro-ph.HE]
[60] K. Moriyama, A. Cruz-Osorio, Y. Mizuno *et al.*, Astron. Astrophys. **694**, A135 (2025), arXiv: 2501.08720[astro-ph.HE]
[61] A. Chael, Mon. Not. Roy. Astron. Soc. **532**, 3198 (2024), arXiv: 2404.01471[astro-ph.HE]
[62] P. Kocherlakota and L. Rezzolla, Mon. Not. Roy. Astron. Soc. **513**, 1229 (2022), arXiv: 2201.05641[gr-qc]
[63] C. M. Fromm *et al.*, Astron. Astrophys. **660**, A107 (2022), arXiv: 2111.02518[astro-ph.HE]
[64] D. Bardiev, Y. Wang, M. Kološ *et al.*, Astrophys. J. **972**, 55 (2024)
[65] D. Bardiev, J. Schee, and Z. Stuchlxık, Astrophys. J. **993**, 62 (2025)
[66] O. Y. Tsupko and G. S. Bisnovatyi-Kogan, Gravit. Cosmol. **15**, 184 (2009)
[67] S. Chandrasekhar, *The Mathematical Theory of Black Holes* (Oxford University Press, 1983)
[68] G. Z. Babar, F. Atamurotov, and A. Z. Babar, Physics of the Dark Universe **32**, 100798 (2021)
[69] S. Vxazquez and E. Esteban, Il Nuovo Cimento B **119**, 489 (2004)
[70] C. Bambi, K. Freese, S. Vagnozzi *et al.*, Phys. Rev. D **100**, 044057 (2019)
[71] K. Akiyama *et al.* (Event Horizon Telescope Collaboration), Astron. Astrophys. **681**, A79 (2024)
[72] M. De Laurentis and P. Salucci, Astrophys. J. **929**, 17 (2022), arXiv: 2206.01997[astro-ph.CO]
[73] R. Abuter *et al.* (GRAVITY), Astron. Astrophys. **636**, L5 (2020), arXiv: 2004.07187[astro-ph.GA]
[74] A. Rogers, Mon. Not. Roy. Astron. Soc. **451**, 17 (2015), arXiv: 1505.06790[gr-qc]
[75] X. Er and A. Rogers, Mon. Not. Roy. Astron. Soc. **475**, 867 (2017), arXiv: 1712.06900[astro-ph.GA]
[76] P. Goldreich and W. H. Julian, Astrophys. J. **157**, 869 (1969)
[77] F. Atamurotov, A. Abdujabbarov, and J. Rayimbaev, Eur. Phys. J. C **81**, 118 (2021)
[78] O. Y. Tsupko and G. S. Bisnovatyi-Kogan, Plasma Physics Reports **41**, 562 (2015)
[79] P. Schneider, J. Ehlers, and E. E. Falco, *Gravitational Lenses*, Astronomy and Astrophysics Library (Heidelberg: Springer Berlin,1992)
[80] F. Atamurotov, K. Jusufi, M. Jamil *et al.*, Phys. Rev. D **104**, 064053 (2021), arXiv: 2109.08150[gr-qc]